"Bio-drop" Evaporation and Ring-Stain Deposits: the Significance of DNA Length

Alexandros Askounis,*[,1,2] Yasuyuki Takata,[1,2] Khellil Sefiane,[2,3] Vasileios Koutsos,*[,3] and Martin E. R. Shanahan[4,5,6]

[1]Department of Mechanical Engineering, Thermofluid Physics Laboratory, Kyushu University, 744 Motooka, Nishi-ku, Fukuoka, 819-0395, Japan

[2]International Institute for Carbon-Neutral Energy Research (WPI-I2CNER), Kyushu University, 744 Motooka, Nishi-ku, Fukuoka 819-0395, Japan

[3]Institute for Materials and Processes, School of Engineering, The University of Edinburgh, King's Buildings, Robert Stevenson Road, Edinburgh, EH9 3FB, United Kingdom.

[4]Univ. Bordeaux, I2M, UMR 5295, F-33400 Talence, France.

[5]CNRS, I2M, UMR 5295, F-33400 Talence, France.

[6]Arts et Métiers ParisTech, I2M, UMR 5295, F-33400 Talence, France.

*To whom correspondence should be addressed: E-mail: a.askounis@i2cner.kyushu-u.ac.jp; Tel.: +81-92-802-3905 Fax: +81-92-802-3905. E-mail: vasileios.koutsos@ed.ac.uk; Tel.: +44 (0)131 650 8704; Fax: +44 (0)131 650 6551

Abstract

Small sessile drops of water containing either long or short strands of DNA ("bio-drops") were deposited on silicon substrates and allowed to evaporate. Initially, the triple line (TL) of both types of droplet remained pinned but later receded. The TL recession mode continued at constant speed until almost the end of drop lifetime for the bio-drops with short DNA strands, whereas those containing long DNA strands entered a regime of significantly lower TL recession. We propose a tentative explanation of our observations based on free energy barriers to unpinning and increases in the viscosity of the base liquid due to the presence of DNA molecules. In addition, the structure of DNA deposits after evaporation was investigated by AFM. DNA self-assembly in a series of perpendicular and parallel orientations was observed near the contact line for the long-strand DNA, while with the short-stranded DNA smoother ring-stains with some nanostructuring but no striations were evident. At the interior of the deposits, dendritic and

faceted crystals were formed from short and long strands respectively; due to diffusion and nucleation limited processes respectively. We suggest that the above results related to the bio-drop drying and nanostructuring are indicative of the importance of DNA length, i.e. longer DNA chains consisting of linearly bonded shorter, rod-like DNA strands.

Introduction

The drying of suspension droplets is at the forefront of scientific activity as a deposition technique for various applications such as bio-sensing DNA microarrays[1] or ink-jet printing for microelectronic devices.[2] However, an important problem with this process is controlling the deposition of the solids on the substrate during evaporation.

In their seminal work, Deegan *et al.* elucidated the underlying physics of the ubiquitous "coffee-stain" deposition phenomenon.[3, 4, 5] Essentially, evaporation with a pinned three-phase contact line (triple line: TL) of a suspension drop containing microparticles induces an outward fluid flow to sustain the liquid front, which in turn carries the dispersed particles to the drop periphery leading to the formation of ring deposits. These deposits have been reported to consist of mainly crystalline structures.[6, 7] Nonetheless, the formation of disordered regions has been reported and attributed, in the case of microspheres, to the rapidly increasing particle velocity near the end of droplet lifetime, allowing little time for Brownian motion;[8] while in the case of nanospheres, to an interplay between particle velocity (this time as an ordering parameter) and wedge constraints (disordering parameter).[9, 10] The addition of slightly elongated particles (aspect ratio 3.5) suppressed the "coffee-stain" mechanism[11] due to the formation of loosely packed aggregates at the liquid-air interface, which in turn create strong capillary attractions

between the aggregates and the incoming ellipsoids, thus reducing their mobility. Longer particles such as carbon nanotubes (CNTs),[12] silica rods[13] or graphene flakes[14] led to "coffee-stains" with different structuring as the wedge constraints weakened.

On the other hand, polymer drop evaporation, which is very important in ink-jet printing technologies,[2] may lead to the formation of a variety of structures: ring-stain,[15, 16, 17] hat-like[16, 17, 18, 19] and "puddle" and/or "pillar".[20, 21, 22] The formation of ring-stains was attributed to the "coffee-stain" phenomenon.[13] Puddles and/or pillars were associated with pinning duration[16, 22] which, when coupled with the formation of a particulate skin at the liquid-vapor interface, led to a buckling instability and the formation of hat-like structures.[18, 19]

The drying of drops of biopolymers, such as DNA, is another interesting area with great promise as it may revolutionize genome expression detection, especially in the form of DNA microarrays.[1] DNA is a biological polymer which consists of a number of monomer units, named base pairs (bp), of the four nucleotides Adenine, Thymine, Guanine, Cytosine.[23] Its shape is regarded to be cylindrical, with *ca*. 2nm diameter and varying in length according to the number of bp, each corresponding to *ca.* 3.4 Å.[23] In spite of its importance, the exact mechanism governing the evaporation of DNA droplets remains elusive.[24] Dugas *et al.* reported the evaporation kinetics and pattern formation of a bio-drop containing oligonucleotides (25 bp DNA strands), which evaporated with an initial pinning period, followed by TL retraction at constant speed.[25] The evaporation of individual bio-drops containing λ- phage DNA (48.5 kbps, *ca.* 16 μm) of increasing concentration showed a transition from constant contact radius (CCR) to constant contact angle

(CCA) evaporation modes.[26] In addition, it was reported that DNA self-assembled into branched structures, whose dimensions were a linear function of DNA concentration.[26]

DNA is capable of self-assembly into a variety of structures. For example, Heim *et al.* reported that λ- phage DNA (48.5 kbp, *ca.* 16 μm) formed branched structures when the bio-drop front moved away from its original location.[27] However, when the droplet front remained pinned, similar DNA strands (48.5 kbp, *ca.* 16 μm) formed zig-zag patterns.[28] On the other hand, very short (2-7 nm)[29] or relatively short (50 nm) DNA strands formed liquid crystals with columnar, nematic or dendritic order depending on DNA concentration.[30] Nonetheless, little is known about the self-assembly process of DNA at the TL of drying drops, especially with numbers of bp between 100 and 1000 or with chain lengths between 34 nm and 340 nm.

Drop drying is a complex multiscale and multiphase, physical phenomenon and many of its aspects still remain elusive. However, it is easy to implement practically and has considerable potential applications, including micro-devices for DNA characterization.[27] In this article, we attempt to bridge a gap in the understanding of the evaporation kinetics of bio-drops containing DNA strands with lengths ranging between 34 - 340 nm and, at the same time, associate the influence of DNA length on both bio-drop evaporation kinetics and deposit growth. In addition, we investigate DNA self-assembly within these deposits.

Materials and Methods

DNA with 100 and 1000 base pairs (bp) (NoLimits™ Individual DNA Fragments), corresponding to lengths of 34 and 340 nm respectively, were acquired from Thermo Scientific (Waltham, MA)

in powder form. The powder was dissolved at 0.01 % w/v concentration with deionized water and stirred using a vortex stirrer until complete dispersion. Smooth ($R_{rms}\sim$ 1 nm) silicon substrates with a thin, native silica surface layer (due to oxidation) were used as substrates in order to minimize contact angle (CA) hysteresis. Substrates were cleaned in an iso-propanol ultrasonic bath for approx. 10 mins, rinsed with deionized water and dried using a jet of compressed air, prior to use. A Krüss DSA100 (Krüss GmbH, Hamburgh, Germany) drop shape analyzer (DSA) system was employed to deposit 3 µL droplets of each solution. The CCD camera (recording at 25 fps) mounted on the DSA allowed acquisition of droplet profile (contact angle, radius and volume) evolution over time. Evaporation experiments were conducted in a room with controlled temperature of 21 ± 2 ℃ and relative humidity between 30% and 40%. A minimum of 10 repetitions of each experiment were conducted in order to establish reproducibility and we provide a representative example of each case. The viscosity of each suspension was measured with an automatic microviscometer (AMVn, Anton Paar GmbH ,Graz, Austria).

Sample imaging was conducted with a Bruker Multimode/ Nanoscope IIIa AFM (Bruker, Santa Barbara, CA). The AFM was equipped with a J-scanner (x-y scan range of approx. 140 microns) and operated under tapping mode (tip in intermediate contact with the surface). Bruker RTESP cantilevers were used with a nominal (according to manufacturer's specification) spring constant of 40 N/m, resonance frequency of 300 kHz and tip curvature of *ca.* 8 nm. Images were post-processed and analyzed using the Scanning Probe Image Processor (SPIP, Image Metrology, Hørsholm, Denmark).

Results and discussion

Representative results of contact angle, θ, and radius, R, *vs.* time for short, 100 bp, and long, 1000 bp, strands are presented in Figure 1(a) and (c). The two cases exhibit similar initial evaporative behavior, in the CCR mode (Stage I). In this mode the TL remains pinned, inducing an outward liquid flow carrying particles to the periphery, which in turn form the rings observed in Figure 1 (b) and (d). When the CA reaches a sufficiently small, threshold value, $\theta = \theta_r$, following TL pinning, the bio-drops are in a state of sufficient excess free energy, with respect to their thermodynamic equilibrium shape, *viz.* corresponding to an equilibrium value of contact angle, in order to overcome the pinning force (or energy barrier) and they enter stage II, where they evaporate in the CCA regime.[31] After further evaporation, both systems enter stage III, although this stage differs for the 100 and 1000 bp cases. In the case of short DNA (Figure 1 (a)), evaporation proceeds under a combination of receding TL and decreasing CA, whereas in the case of longer DNA strands (Figure 1 (c)), evaporation enters what is virtually a second CCR mode prior to complete evaporation, although some slight decrease in contact radius does occur. These results are in agreement with what has been reported for drying of bio-drops containing much longer DNA chains, length of 48.5 kbp or *ca.*16μm.[26] This behavior for 1000 bp is similar to that observed for a suspension of TiO_2 particles in ethanol.[32] Although the TL barely moves, there is a perceptible drift towards lower values of contact radius.

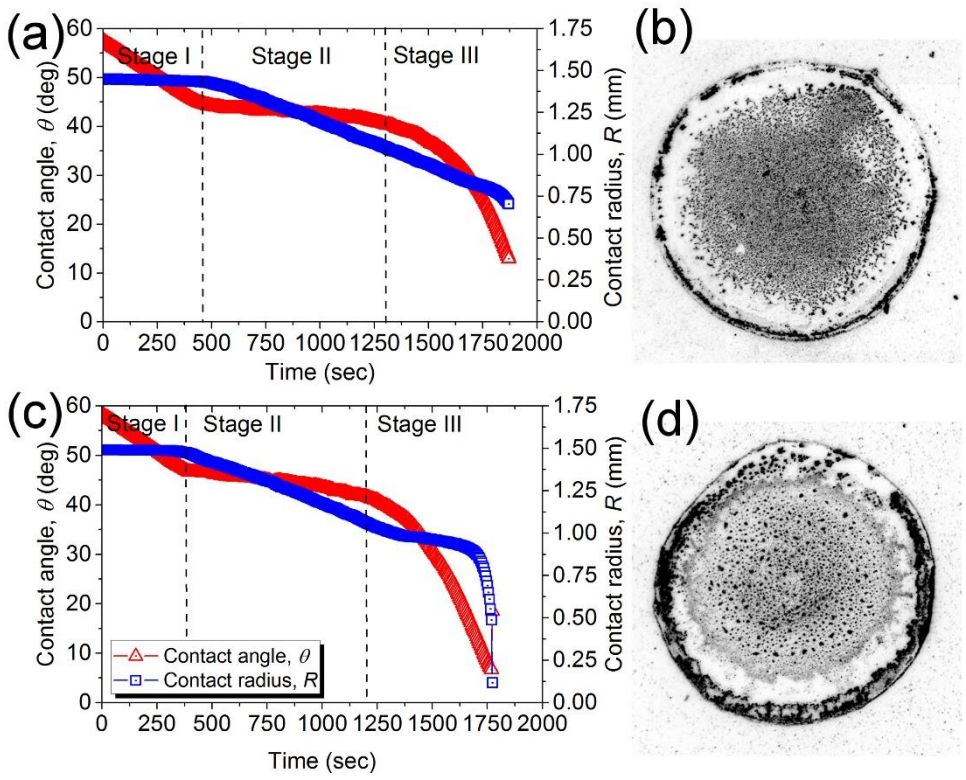

Figure 1. (a) Representative contact angle and contact radius *vs* evaporation time of 3 µl aqueous droplets containing 0.01 % w/v (a) 100 bp and (c) 1000 bp DNA chains. (b), (d) Corresponding optical micrographs of the ring-stain deposits left behind after the free evaporation each solution.

Consideration of the evaporation behavior of these two types of bio-drop reveals two interesting points about the effect of particle (strand) length on evaporation kinetics. Firstly, the shorter DNA strands lead to stronger, initial TL pinning, as indicated by a longer pinning period (*ca.* 460 ± 22 sec, compared to the longer strands, *ca.* 380 ± 19 sec.) and (slightly) lower contact angle at depinning (44° compared to 47°). This is in agreement with results previously reported for rigid, rod-like solid particles CNTs[14] or silica rods.[13] In these bio-drops, this rod-like behavior of the short DNA strands may be explained by considering simple polymer physical properties, *i.e.* the persistence length, which is, essentially, a way of classifying the stiffness of polymers. In

the case of DNA, the persistence length was reported to be *ca.* 50 nm or 150 bp.[28, 29, 33] Therefore, our 100 bp DNA strands may be regarded as essentially rigid and exhibiting rod-like behavior similar to CNTs.[14] On the other hand, the longer, 1000 bp, DNA strands may be considered as 10 short rods linked linearly by chemical bonds. This bonding imposes a constraint in the possible conformations of each individual short rod. Additionally, this bonding leads to fewer (larger) individual solute molecules (for a given mass concentration), leading to weaker TL pinning.

The second interesting point arising from the comparison of the evaporative behavior of the two types of bio-drops in Figure 1 is the difference in recession speeds of the TL. Average droplet recession speeds during Stage II were calculated from a series of experiments to be: $v_{short} \approx 4.9\times10^{-7} \pm 1.9\times10^{-7} m/\sec$ and $v_{long} \approx 3.7\times10^{-7} \pm 4.5\times10^{-8} m/\sec$ for the short and long DNA, respectively. It is worthwhile noting that even a very small amount of solute accumulation at the drop edge is capable of slowing down a moving contact line.[34] The difference in TL recession rate of the two bio-drops may be attributed to the longer chain length leading to higher, local, viscosity at the TL, consistent with polymer[34, 35] or biopolymers.[36] The dynamic viscosities of the two suspensions (at initial concentrations) were measured to be $\eta_{short} =$ 0.880 mPa·s and $\eta_{long} =$ 0.921 mPa·s, corresponding to relative viscosities of $\eta_{r,short} =$ 1.078 and $\eta_{r,long} =$ 1.129 with respect to water ($\eta_{water} =$ 0.816 mPa·s measured at the same conditions). The concentration locally at the TL is expected to increase due to solvent evaporation, which results in even higher viscosities.

As a sessile drop evaporates at constant contact radius, its contact angle decreases below the Young (or equilibrium) value and the system becomes unequilibrated thermodynamically,

leading to an excess of free energy, δG. With knowledge of both θ and R at any given time, we can calculate the evolution of this excess free energy, $G(\theta)$, over the equilibrium value, $G(\theta_0)$, as $\delta G = G(\theta) - G(\theta_0)$ which leads to Equation 1:[9]

$$\delta G = \frac{\gamma \pi R^2}{(1+\cos\theta)}[2 - \cos\theta_0(1+\cos\theta) -$$

$$-(1-\cos\theta)^{1/3}(2+\cos\theta)^{2/3}(2+\cos\theta_0)^{1/3}(1-\cos\theta_0)^{2/3}] \qquad (1),$$

where θ_0 is the initial CA (assumed to be the Young value: see below) and γ is the solution surface tension, measured in independent experiments by the pendant drop technique to be that of pure water, *ca.* 0.073 N/m. Dividing δG by droplet circumference, we calculate the excess free energy per unit length of TL, $\delta \bar{G} = \delta G / 2\pi R$. Results of $\delta \bar{G}$ *vs* normalized time, *i.e.* time, t/drop lifetime, t_{max}, are plotted in Figure 2 for the two types of bio-drop, containing either short or long DNA strands.

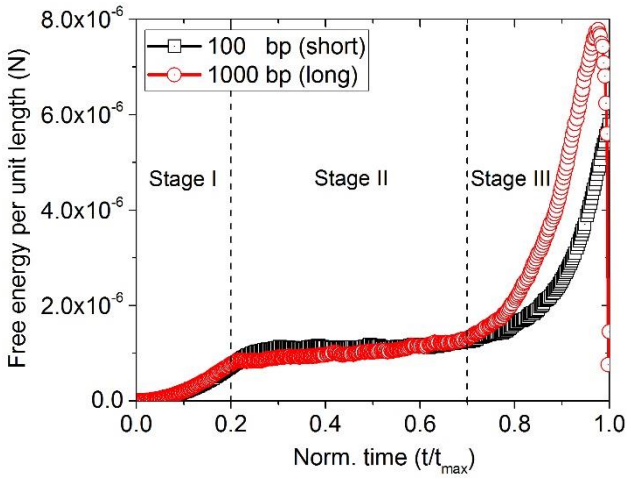

Figure 2. Comparison of the evolution of free energy per unit length, $\boldsymbol{\delta\bar{G}}$, evolution of short – 100 bp (squares) and long – 1000 bp (circles) DNA strands.

The variation in $\delta\bar{G}$ appears generally to follow a similar trend in both systems. Initially, excess free energy increases during the CCR mode of evaporation (stage I of Figure 1). Upon $\delta\bar{G}$ reaching the threshold depinning energy, at *ca.* 20 % of drop lifetime, $\delta\bar{G}_{short} \approx 1.1 \times 10^{-6}\, N$, for the 100 bp DNA (squares) and $\delta\bar{G}_{long} \approx 8.6 \times 10^{-7}\, N$, for the 1000 bp (circles), a jump occurs and then $\delta\bar{G}$ exhibits a plateau, which is indicative of a quasi-equilibrium during TL retraction. (The fact that $\delta\bar{G}$ is calculated to be non-zero at this stage sheds doubt on the above assumption that the initial CA is the true Young angle, but this is of little importance in the argument, relative values of $\delta\bar{G}$ being considered, as also pointed out elsewhere.[37]) Towards *ca*. 70% of drop lifetime, a relatively rapid increase in $\delta\bar{G}$ begins, more marked for the 1000 bp case. This corresponds to the onset of significant reduction in CA (see Figure 1). The fact that $\delta\bar{G}$ attains (relatively) high values, $\delta\bar{G}_{short} \approx 5.7 \times 10^{-6}\, N$ and $\delta\bar{G}_{long} \approx 7.7 \times 10^{-6}\, N$, suggests that any potential depinning of the TL to attempt to restore Young equilibrium is severely hindered.

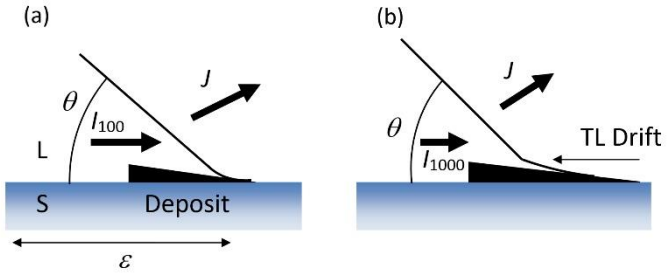

Figure 3. Schematic representation of TL region, where ε is a cut-off to local behavior. (a) For lower viscosity suspension (100 bp), liquid flux, I_{100}, is capable of supplying the needs of

evaporation (flux J) to maintain continuity and CA remains relatively large. (b) For higher viscosity (1000 bp), liquid flux is inadequate for the needs of evaporation, CA diminishes, drop flattens locally and TL drifts due to higher viscosity.

Since in both cases, with DNA strands of 100 and 1000 bp, there is some motion of the TL (Stage I of Figure 1), albeit slight for 1000 bp, we cannot consider the effect as being due to an energy *barrier*, *per se*, but to a kinetic (or dynamic) effect. If some TL drift occurs during the deposition process, it has been shown that the evaporation deposit may adopt the form of a wedge of thin end facing the exterior of the drop[32] (see Figure 3). The wedge was found to be reasonably modelled by the expression:

$$h(x) \approx \frac{f_i \bar{J} \varepsilon}{\rho_s \dot{R}} \left(1 + \frac{2\bar{J}x}{R\rho_l \varepsilon \sin\theta} \right) \qquad (2),$$

where $h(x)$ is wedge height as a function of distance, x, measured from the TL towards the drop centre, f_i is the initial concentration of suspension particles, $\bar{J}$ the average evaporative flux near the TL, taken up to some limiting (small) distance, ε, $\dot{R}$ is TL drift speed, ρ_s and ρ_l are respectively solid (the suspension, in the form found in the deposit) and liquid densities, and θ is contact angle. Although unknown with any precision, ε was found to be of the order of 100 nm.[32] Equation 2 reveals the physical mechanism underlying the deposit build-up and may provide a plausible explanation of the differences observed between the two bio-drops shown in Figure 1. In the absence of any significant viscosity, this description seems to be adequate provided that the liquid replenishment flux, I, is sufficient to maintain continuity with the

(governing) evaporation flux, $\bar{J}$. Under these conditions, liquid viscosity plays no role in deposit build-up (Figure 3(a)) and does not appear in Equation (2), as would appear to be the case for the shorter DNA strands with $I = I_{100}$. However, if the viscosity of the suspension is higher (as in the longer DNA case), the liquid flux may be unable to replenish the depletion caused by local evaporation near the TL, leading to stagnation of the process, flattening of the local liquid layer and subsequently to a more rapid drop in the CA (Figure 3(b)). The TL will then recede at a lower rate, as discussed above. Thus the discontinuity between available liquid input and evaporation loss will lead to both a more rapidly decreasing CA and a slower recession of the TL. Indeed Figure 2 quite clearly shows that the energy barrier in Stage III is considerably higher for 1000 bp than for 100 bp. To support this argument further, we provide in Figure 4 the comparison of the average radial light intensity profiles of the deposits presented in Figure 1. Integration of the area under the curves reveals an increase in ring area with the DNA length from $13.1 \pm 3.1\%$ to $31.2 \pm 5.0\%$ of the total area. This amounts to a ca. threefold increase in ring width with increased viscosity, due to higher DNA length. Potentially, this crude comparison could prove to be a quick and inexpensive way to categorize DNA strands according to their length, similar to other biomedical applications for drop drying such as blood diagnosis.[38, 39] Nonetheless, further examination is required in this direction.

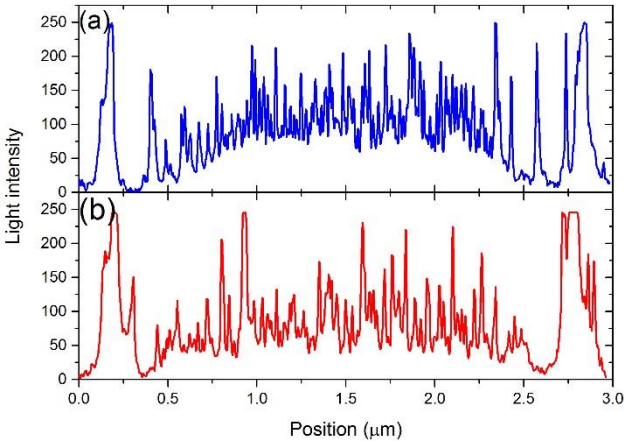

Figure 4: Average light intensity profiles of ring-stains left behind the evaporation of (a) 100 bp and (c) 1000 bp bio-drops.

The effect of DNA length on nanostructuring within the ring-stains was also investigated. We imaged the resulting patterns (Figure 1 (b), (d)) with AFM mainly at two areas where nano-

structuring behaviour has been reported previously: at the outer edge of the ring-stain (TL)[7, 9, 11, 14, 40] and towards the interior of the resulting patterns (towards the drop bulk).[8, 10, 41]

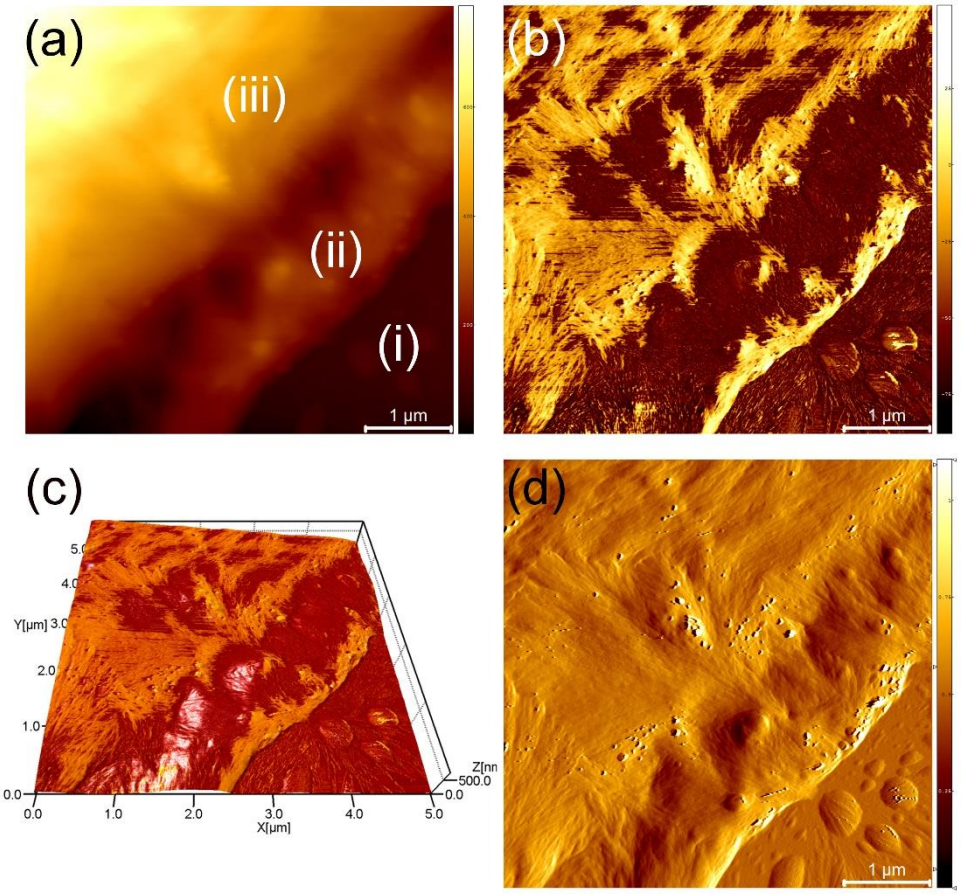

Figure 5. (a) 5 × 5 µm^2 topography image of the edge of the deposit (TL) left behind after the evaporation of the droplet containing long – 1000 bp DNA, z-scale ranges 0 – 770 nm. (b) Phase image of the same area, z-scale ranges -80° – 35°. (c) 3-D representation combining information from both (a) and (b). (d) Amplitude image of the same area, z-scale ranges -200 – 200 mV.

Figure 5 depicts the topography (a) and the phase image (b) of the outer edge of the 1000 bp ring-stain. The phase image shows tip-sample interactions due to viscoelasticity, adhesion or

even different particulate orientation and therefore provides better contrast in DNA nanostructuring. Figure 5 (c) shows a 3-D representation of (a) with an overlay of (b). Moreover, we provide the amplitude image of the same area in Figure 5 (d), which is essentially the error-signal of the AFM feedback loop and provides better contrast. Some particulate deposited on the substrate can be identified outside the ring (area (i)), attributable to an initial, rapid dewetting occurring directly after droplet deposition on the substrate. Noticeably, in the same area, the DNA strands seem to have oriented with the flow due to the rapid TL motion stretching the molecules.[26, 27] Inside the ring-stain and near the TL (area (ii)), a *ca.* 1.60 µm wide plateau was formed. The formation of this plateau may be attributed to insufficient particulate supply from the periphery as a result of the viscosity of this droplet which in turn is enhanced at the wedge (as discussed above). Moving away from the periphery there is more volume available and hence lower viscosity which allows the particulate supply to resume and hence the deposit to grow again. Notably, the DNA strands self-assembled within the deposit (area (ii)) mainly parallel to the edge of the ring in order to achieve the densest possible packing. However, some DNA strands appear to be perpendicular to the edge, potentially due to the TL retraction forcing them to align with its motion. Similar undulations of DNA chains were reported to have formed during the retraction of the TL of DNA droplets; albeit containing much larger DNA strands (16 µm compared to 340 nm here, $\sim 50\times$ larger), observed with confocal microscopy.[28] This plateau is followed by area (iii) where a distinctive step can be observed and strands with similar nanostructuring, mainly parallel with a few perpendicular to the TL, hinting perhaps at another, smaller TL pinning event, not detectable by the CCD camera. Further away from the TL and toward the ring interior (top left corner of Figure 5 (b)), DNA strands are free to orient to the flow, due to weaker wedge constraints, and the DNA strands exhibit a mixture of parallel and perpendicular orientation to the TL.

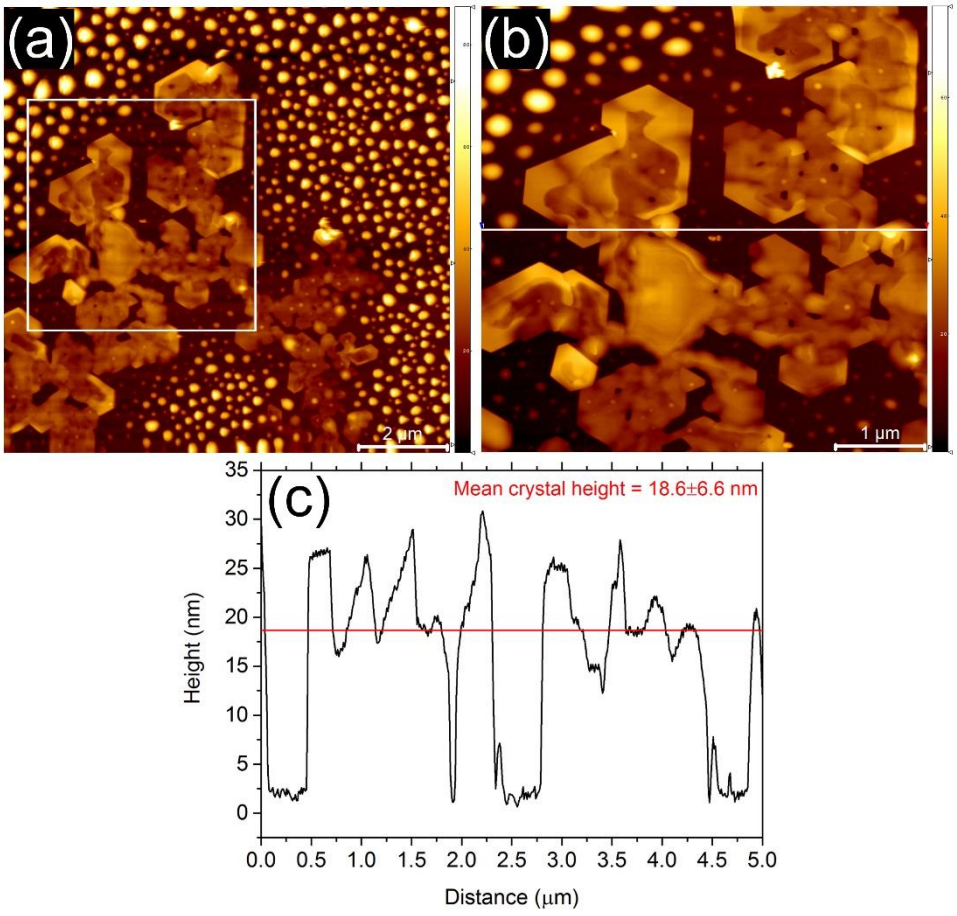

Figure 6. (a) 10.0 × 10.0 µm^2 topography image of the central area of the 1000 bp pattern, z-scale ranges 0 – 90 nm. (b) 5 × 5 µm^2 magnification of the area in the white box in (a), z-scale ranges 0 – 80 nm. (c) Mean height profile corresponding to line in (b).

At the interior of the deposit, the 1000 bp DNA strands exhibit a different structuring behavior, depicted in the topography image in Figure 6 (a). A series of spherical cap particulate islands were found to have formed randomly on the substrate. These islands are characteristic of pseudo-dewetting structures (as the surface is still covered by liquid/particulate).[42, 43, 44] As these islands grow they will merge, eventually, giving rise to the network with the sharp edges highlighted by the white box in Figure 6 (a) and magnified for better inspection in Figure 6 (b).

This crystallization can be attributed to “faceted growth”, which is essentially a nucleation-limited process.[45, 46] From Figure 6 (b), it is readily apparent that the lateral dimensions of the facets varied. However, their height is relatively uniform, as shown in the average height profile in Figure 6 (b), with a typical average value of 18.6 ± 6.6 nm.

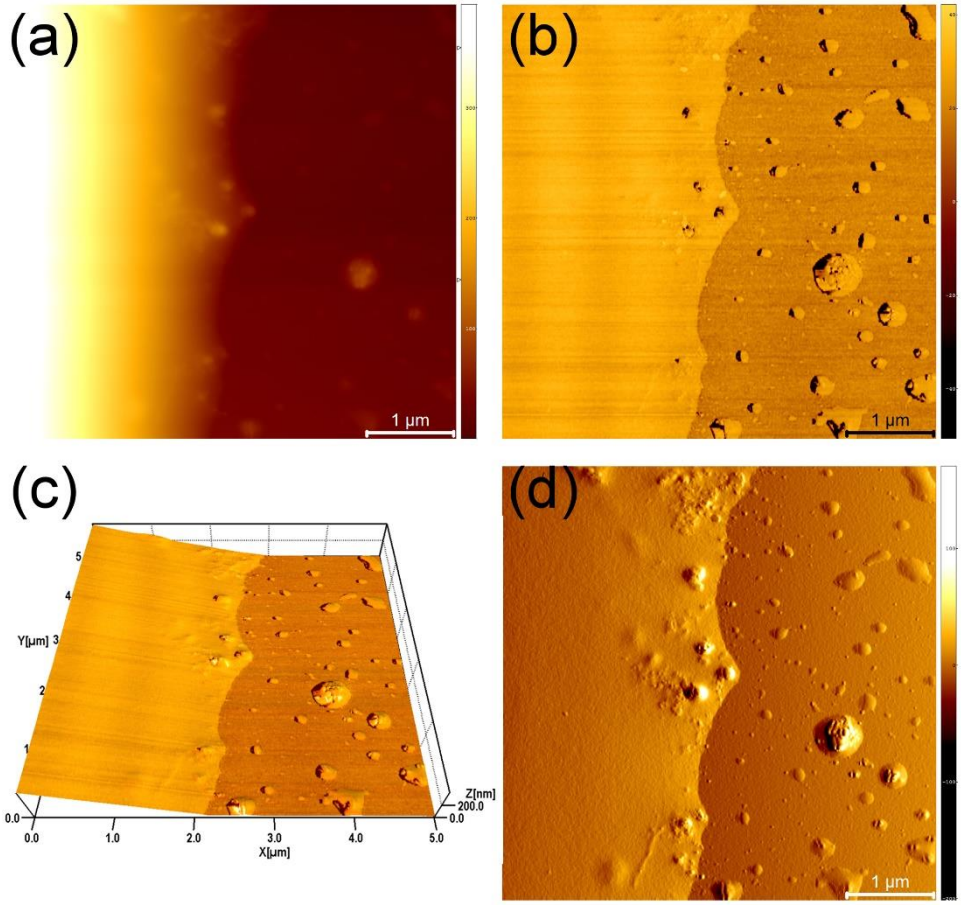

Figure 7. (a) 5 × 5 µm^2 topography image of the edge of the deposit (TL) left behind after the evaporation of the droplet containing short– 100 bp DNA chains, z-scale ranges 0 – 380 nm. (b) Phase image of the same area, z-scale ranges -50^o – 40^o. (c) 3-D representation combining information from both (a) and (b). (c) 3-D representation of the same area. (d) Amplitude image of the same area, z-scale ranges -200 – 200 mV.

Figure 7 (a) depicts the topographical information of the outer edge of the bio-drop containing short DNA chains and Figure 7 (b) depicts the phase image of the same area. Combining the information of both these images results in the three-dimensional representation of the same area presented in Figure 7 (c). Outside the ring, on the right hand side of the images, a number of large, spherical cap particulate islands can be identified. These islands could be attributed to an initial dewetting event occurring directly after the droplet was deposited on the substrate, which was too rapid for the CCD camera to capture and show in Figure 1 (a). This argument is further supported by the presence of similar large, particulate aggregates within and near the outer edge of the deposit. These aggregates, however, were possibly formed around/ on top of surface defects which led to the anchoring of the TL. In addition, some DNA nanostructures were found to have formed around these larger aggregates and a larger fibril near the bottom, which are clearly identifiable in the amplitude image shown in Figure 7 (d). Overall, we can only surmise at this point that the 100 bp DNA strands formed a rather smooth coffee-stain deposit without striations. Furthermore, the slope of this ring-stain appears to have grown steadily (without any steps) and therefore sharper than in the longer – 1000 bp case. This difference could perhaps be attributed to lower viscosity in the 100 bp droplet (as discussed above); short DNA strands are not linked linearly via chemical bonds and thus can move more easily and independently allowing a steady flow of particles arriving to the wedge and leading to the continuous deposit growth.

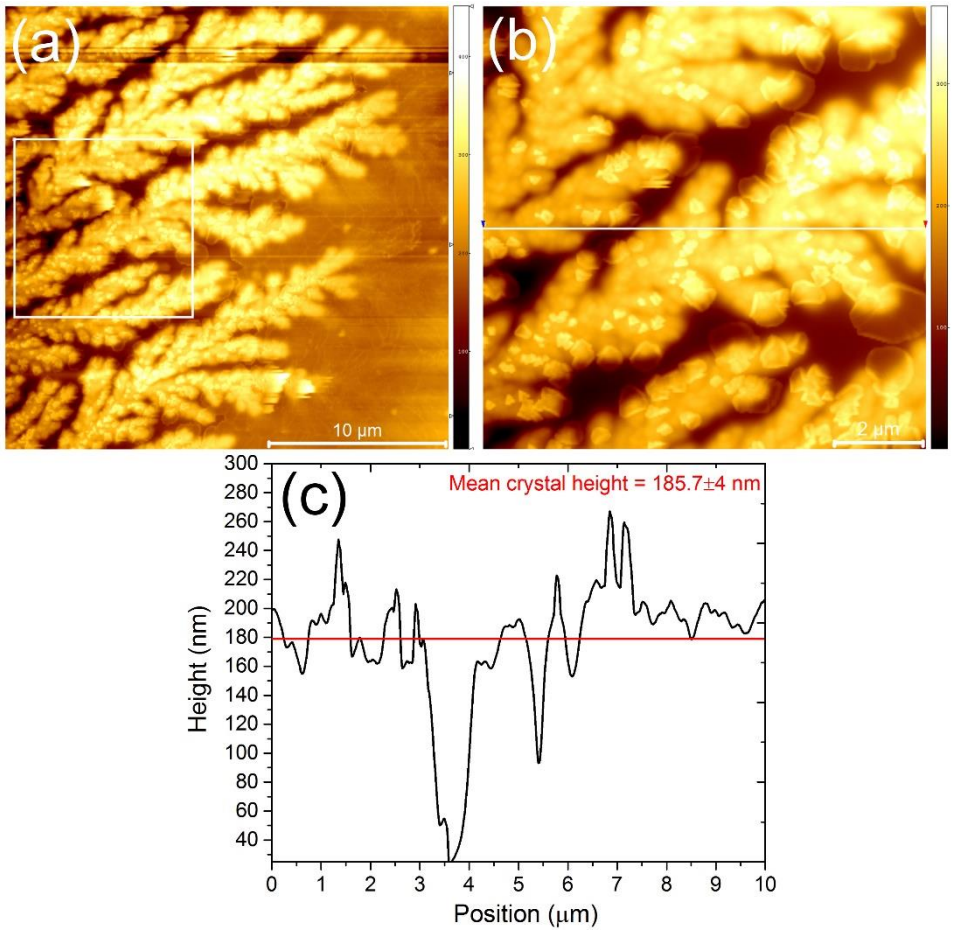

Figure 8. (a) 25.0 × 25.0 µm^2 topography image of the central area 100 bp pattern, z-scale ranges 0 – 370 nm. (b) 10 × 10µm^2 magnification of the area in the white box in (a), z-scale ranges 0 – 330 nm. (c) Mean height profile corresponding to line in (b).

A typical topography image of the area towards the center of the 100 bp deposit shows the formation of dendritic structures (Figure 8 (a)). The dendrites propagated from the drop center (toward the left hand side of the image). Similar DNA dendrites have been reported in the past, albeit for much smaller DNA strands *ca.* 8 bp.[29] The close-up of the dendrites presented in Figure 8 (b) allows better inspection of the structures and the determination of their average height to be *ca.* 186 ± 25 nm. This average height profile presented in Figure 8 (c) was acquired from a

number of height profiles, a representative one being shown in Figure 8 (b). From these results we may hypothesize on the crystallization process mechanism. Potentially, some DNA strands may be adsorbed at the solid-liquid interface where they act as nucleation sites, giving rise to dendrite crystals, following diffusion-limited crystal growth.[45] In addition, comparing the crystals in Figure 6 and Figure 8 leads to the conclusion that the crystallization process is highly dependable on DNA length and mobility.

Conclusions

We have studied the evaporation of bio-drops containing DNA strands of 100 and 1000 bp. Evaporation behavior, coffee-stain formation and nano-structuring were found to be dependent on DNA strand length and are also indicative of a link between DNA viscosity and evaporation behavior. Suspensions of DNA of both chain lengths exhibited a three-stage evaporation cycle; the major difference occurring at stage III, *viz*. after initial CCR and subsequent CA behavior. The initial CCR period is slightly longer for the short DNA strand suspension, probably due to more efficient/denser packing behavior of the short strands and hence stronger pinning. Upon depinning, both bio-drops retract with the longer strand version retracting at a slower rate. Eventually, evaporation enters a third mode of evaporation, different for each case. The short strand suspension follows with a combination of decreasing CA and retracting TL. On the other hand, the longer strand DNA suspension enters a second CCR mode. Both the lower retraction rate and second CCR evaporation cycle of the longer strand case were attributed to higher local viscosity at the TL, modifying the overall local flow/evaporation process. Essentially, the more efficient/denser packing of the short DNA leads to higher energy requirements for the first depinning event to occur, whereas the higher viscosity near the end of droplet life leads to stronger contact angle hysteresis for the longer DNA and hence to a second CCR event.

Nanoscale investigation of the edge of the resulting ring deposits unveiled more information about the evaporation process. There appears to be an initial dewetting stage in both cases, which was apparently too rapid or too small (AFM images exhibit areas of a few μm) to be captured by our CCD camera. Upon the TL meeting a surface defect, the rod-like, short DNA strands accumulated there, giving rise to strong pinning of the TL. On the other hand, the longer DNA strands exhibit unique nanostructuring behavior. Near the TL, long DNA strands tend to pack themselves as densely as possible in the limited wedge space with the occasional stretching due to some random anchoring points. Moving towards the interior of the ring, where the wedge constraints are weaker, DNA chains exhibit a higher conformation to liquid flow, giving rise to a mixture of parallel and perpendicular orientations with respect to the TL. Towards the center of the resulting patterns (drop side of TL), a unique, crystallization pattern was observed for each DNA strand length. The two DNA strands followed different crystallization paths possibly due to their different degrees of flexibility. We believe that these findings may provide useful information for further development of biomedical applications such DNA microarrays.[1]

Acknowledgements

We gratefully acknowledge the Eric Birse Charitable Trust (J24204) for financial support and the Japanese Society for the Promotion of Science (JSPS) for the Postdoctoral Fellowship for North American and European Researchers. This work has been conducted under the umbrella of COST Action MP1106: Smart and green interfaces.

References

1. Brown, P. O.; Botstein, D. Exploring the new world of the genome with DNA microarrays. *Nature Genetics* **1999,** *21*, 33 - 37.
2. Sirringhaus, H.; Kawase, T.; Friend, R. H.; Shimoda, T.; Inbasekaran, M.; Wu, W.; Woo, E. P. High-Resolution Inkjet Printing of All-Polymer Transistor Circuits. *Science* **2000,** *290* (5499), 2123-2126.
3. Deegan, R. D.; Bakajin, O.; Dupont, T. F.; Huber, G.; Nagel, S. R.; Witten, T. A. Capillary flow as the cause of ring stains from dried liquid drops. *Nature* **1997,** *389* (6653), 827-829.
4. Deegan, R. D. Pattern formation in drying drops. *Phys. Rev. E* **2000,** *61* (1), 475-485.
5. Deegan, R. D.; Bakajin, O.; Dupont, T. F.; Huber, G.; Nagel, S. R.; Witten, T. A. Contact line deposits in an evaporating drop. *Phys. Rev. E* **2000,** *62* (1), 756-765.
6. Shmuylovich, L.; Shen, A. Q.; Stone, H. A. Surface morphology of drying latex films: Multiple ring formation. *Langmuir* **2002,** *18* (9), 3441-3445.
7. Monteux, C.; Lequeux, F. Packing and Sorting Colloids at the Contact Line of a Drying Drop. *Langmuir* **2011,** *27* (6), 2917-2922.
8. Marín, A. G.; Gelderblom, H.; Lohse, D.; Snoeijer, J. H. Order-to-Disorder Transition in Ring-Shaped Colloidal Stains. *Phys. Rev. Lett.* **2011,** *107* (8), 085502-085505.
9. Askounis, A.; Sefiane, K.; Koutsos, V.; Shanahan, M. E. R. Structural transitions in a ring stain created at the contact line of evaporating nanosuspension sessile drops. *Phys. Rev. E* **2013,** *87* (1), 012301.
10. Askounis, A.; Sefiane, K.; Koutsos, V.; Shanahan, M. E. R. The effect of evaporation kinetics on nanoparticle structuring within contact line deposits of volatile drops. *Colloids Surf. A* **2014,** *441*, 855-866.
11. Yunker, P. J.; Still, T.; Lohr, M. A.; Yodh, A. G. Suppression of the coffee-ring effect by shape-dependent capillary interactions. *Nature* **2011,** *476* (7360), 308-311.
12. Small, W. R.; Walton, C. D.; Loos, J.; in het Panhuis, M. Carbon Nanotube Network Formation from Evaporating Sessile Drops. *J. Phys. Chem. B* **2006,** *110* (26), 13029-13036.
13. Dugyala, V. R.; Basavaraj, M. G. Evaporation of Sessile Drops Containing Colloidal Rods: Coffee-Ring and Order–Disorder Transition. *J. Phys. Chem. B* **2015,** *119* (9), 3860-3867.
14. Askounis, A.; Sefiane, K.; Koutsos, V.; Shanahan, M. E. R. Effect of particle geometry on triple line motion of nano-fluid drops and deposit nano-structuring. *Adv. Colloid Interface Sci.* **2015,** *222*, 44-57.
15. Kajiya, T.; Kaneko, D.; Doi, M. Dynamical Visualization of “Coffee Stain Phenomenon” in Droplets of Polymer Solution via Fluorescent Microscopy. *Langmuir* **2008,** *24* (21), 12369-12374.
16. Fukai, J.; Ishizuka, H.; Sakai, Y.; Kaneda, M.; Morita, M.; Takahara, A. Effects of droplet size and solute concentration on drying process of polymer solution droplets deposited on homogeneous surfaces. *Int. J. Heat Mass Transfer* **2006,** *49* (19–20), 3561-3567.
17. Kim, J.H.; Park, S.B.; Kim, J. H.; Zin, W.C. Polymer Transports Inside Evaporating Water Droplets at Various Substrate Temperatures. *J. Phys. Chem. C* **2011,** *115* (31), 15375-15383.
18. Pauchard, L.; Allain, C. Buckling instability induced by polymer solution drying. *EPL (Europhysics Letters)* **2003,** *62* (6), 897.
19. Pauchard, L.; Allain, C. Stable and unstable surface evolution during the drying of a polymer solution drop. *Phys. Rev. E* **2003,** *68* (5), 052801.
20. Baldwin, K. A.; Granjard, M.; Willmer, D. I.; Sefiane, K.; Fairhurst, D. J. Drying and deposition of poly(ethylene oxide) droplets determined by Peclet number. *Soft Matter* **2011,** *7* (17), 7819-7826.

21. Baldwin, K. A.; Fairhurst, D. J. The effects of molecular weight, evaporation rate and polymer concentration on pillar formation in drying poly(ethylene oxide) droplets. *Colloids Surf. A* **2014,** *441*, 867-871.
22. Mamalis, D.; Koutsos, V.; Sefiane, K.; Kagkoura, A.; Kalloudis, M.; Shanahan, M. E. R. Effect of Poly(ethylene oxide) Molecular Weight on the Pinning and Pillar Formation of Evaporating Sessile Droplets: The Role of the Interface. *Langmuir* **2015,** *31* (21), 5908-5918.
23. Calladine, C. R.; Drew, H. R. *Understanding DNA: the molecule & how it works*; Elsevier Academic Press: San Diego, **1997**.
24. Blossey, R.; Bosio, A. Contact Line Deposits on cDNA Microarrays: A "Twin-Spot Effect". *Langmuir* **2002,** *18* (7), 2952-2954.
25. Dugas, V.; Broutin, J.; Souteyrand, E. Droplet Evaporation Study Applied to DNA Chip Manufacturing. *Langmuir* **2005,** *21* (20), 9130-9136.
26. Fang, X.; Li, B.; Petersen, E.; Seo, Y. S.; Samuilov, V. A.; Chen, Y.; Sokolov, J. C.; Shew, C. Y.; Rafailovich, M. H. Drying of DNA Droplets. *Langmuir* **2006,** *22* (14), 6308-6312.
27. Heim, T.; Preuss, S.; Gerstmayer, B.; Bosio, A.; Blossey, R. Deposition from a drop: morphologies of unspecifically bound DNA. *J. Phys.: Condens. Matter* **2005,** *17* (9), S703.
28. Smalyukh, I. I.; Zribi, O. V.; Butler, J. C.; Lavrentovich, O. D.; Wong, G. C. L. Structure and Dynamics of Liquid Crystalline Pattern Formation in Drying Droplets of DNA. *Phys. Rev. Lett.* **2006,** *96* (17), 177801.
29. Nakata, M.; Zanchetta, G.; Chapman, B. D.; Jones, C. D.; Cross, J. O.; Pindak, R.; Bellini, T.; Clark, N. A. End-to-End Stacking and Liquid Crystal Condensation of 6– to 20–Base Pair DNA Duplexes. *Science* **2007,** *318* (5854), 1276-1279.
30. Livolant, F.; Levelut, A. M.; Doucet, J.; Benoit, J. P. The highly concentrated liquid-crystalline phase of DNA is columnar hexagonal. *Nature* **1989,** *339* (6227), 724-726.
31. Shanahan, M. E. R. Simple Theory of "Stick-Slip" Wetting Hysteresis. *Langmuir* **1995,** *11* (3), 1041-1043.
32. Askounis, A.; Orejon, D.; Koutsos, V.; Sefiane, K.; Shanahan, M. E. R. Nanoparticle deposits near the contact line of pinned volatile droplets: size and shape revealed by atomic force microscopy. *Soft Matter* **2011,** *7* (9), 4152-4155.
33. Hagerman, P. J. Flexibility of DNA. *Annu. Rev. Biophys.* **1988,** *17* (1), 265-286.
34. Monteux, C.; Elmaallem, Y.; Narita, T.; Lequeux, F. Advancing-drying droplets of polymer solutions: Local increase of the viscosity at the contact line. *EPL (Europhysics Letters)* **2008,** *83* (3), 34005.
35. Eales, A. D.; Routh, A. F.; Dartnell, N.; Simon, G. Evaporation of pinned droplets containing polymer – an examination of the important groups controlling final shape. *AIChE J.* **2015,** *61* (5), 1759-1767.
36. Early, T. A.; Kearns, D. R. 1H nuclear magnetic resonance investigation of flexibility in DNA. *Proc. Natl. Acad. Sci. U.S.A.* **1979,** *76* (9), 4165-4169.
37. Oksuz, M.; Erbil, H. Y. Comments on the Energy Barrier Calculations during "Stick–Slip" Behavior of Evaporating Droplets Containing Nanoparticles. *J. Phys. Chem. C* **2014,** *118* (17), 9228-9238.
38. Sefiane, K. On the Formation of Regular Patterns from Drying Droplets and Their Potential Use for Bio-Medical Applications. *Journal of Bionic Engineering* **2010,** *7,* 82-93.
39. Brutin, D.; Sobac, B.; Loquet, B.; Sampol, J. Pattern formation in drying drops of blood. *J. Fluid Mech.* **2011,** *667*, 85-95.
40. Abkarian, M.; Nunes, J.; Stone, H. A. Colloidal Crystallization and Banding in a Cylindrical Geometry. *J. Am. Chem. Soc.* **2004,** *126* (19), 5978-5979.

41. Carle, F.; Brutin, D. How Surface Functional Groups Influence Fracturation in Nanofluid Droplet Dry-Outs. *Langmuir* **2013,** *29* (32), 9962-9966.
42. Hare, E. F.; Zisman, W. A. Autophobic Liquids and the Properties of their Adsorbed Films. *J. Phys. Chem.* **1955,** *59* (4), 335-340.
43. Reiter, G.; Sommer, J. U. Crystallization of Adsorbed Polymer Monolayers. *Phys. Rev. Lett.* **1998,** *80* (17), 3771-3774.
44. Kalloudis, M.; Glynos, E.; Pispas, S.; Walker, J.; Koutsos, V. Thin Films of Poly(isoprene-b-ethylene Oxide) Diblock Copolymers on Mica: An Atomic Force Microscopy Study. *Langmuir* **2013,** *29* (7), 2339-2349.
45. Zhang, G.; Jin, L.; Ma, Z.; Zhai, X.; Yang, M.; Zheng, P.; Wang, W.; Wegner, G. Dendritic-to-faceted crystal pattern transition of ultrathin poly(ethylene oxide) films. *J. Chem. Phys.* **2008,** *129* (22), 224708.
46. Zhang, G.; Zhai, X.; Ma, Z.; Jin, L.; Zheng, P.; Wang, W.; Cheng, S. Z. D.; Lotz, B. Morphology Diagram of Single-Layer Crystal Patterns in Supercooled Poly(ethylene oxide) Ultrathin Films: Understanding Macromolecular Effect of Crystal Pattern Formation and Selection. *ACS Macro Lett.* **2011,** *1* (1), 217-221.

Table of contents graphic